ACS Chemical Neuroscience

Research Article

pubs.acs.org/chemneuro

Microscopic Visualization of Metabotropic Glutamate Receptors on the Surface of Living Cells Using Bifunctional Magnetic Resonance Imaging Probes

Anurag Mishra,*[,†,∥] Ritu Mishra,[‡] Sven Gottschalk,[§,∥] Robert Pal,[†] Neil Sim,[†] Joern Engelmann,[§] Martin Goldberg,[‡] and David Parker*[,†]

[†]Department of Chemistry and [‡]School of Biological and Biomedical Sciences, Durham University, South Road, Durham DH1 3LE, England

[§]High Field MR Centre, Max Planck Institute for Biological Cybernetics, Spemannstrasse 41, Tuebingen 72076, Germany

Supporting Information

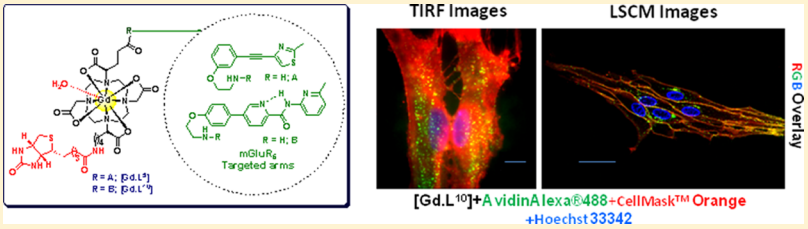

ABSTRACT: A series of bimodal metabotropic glutamate-receptor targeted MRI contrast agents has been developed and evaluated, based on established competitive metabotropic Glu receptor subtype 5 ($mGluR_5$) antagonists. In order to directly visualize $mGluR_5$ binding of these agents on the surface of live astrocytes, variations in the core structure were made. A set of gadolinium conjugates containing either a cyanine dye or a fluorescein moiety was accordingly prepared, to allow visualization by optical microscopy *in cellulo*. In each case, surface receptor binding was compromised and cell internalization observed. Another approach, examining the location of a terbium analogue via sensitized emission, also exhibited nonspecific cell uptake in neuronal cell line models. Finally, biotin derivatives of two lead compounds were prepared, and the specificity of binding to the $mGluR_5$ cell surface receptors was demonstrated with the aid of their fluorescently labeled avidin conjugates, using both total internal reflection fluorescence (TIRF) and confocal microscopy.

KEYWORDS: *$mGluR_5$, imaging agents, lanthanides, MRI, microscopy*

The human brain is a complex system in both intuitive and computational terms. It is involved in the processing of cognitive, sensory, and motor information via neurons which are one of the basic building blocks of the nervous system.[1,2] Chemical neurotransmitters are involved in signal transmission through neurons. One of the active chemical messengers, glutamate (Glu), is abundantly distributed in the mammalian central nervous system (CNS), and plays a critical role in mediating excitatory signals through both G-protein-coupled metabotropic receptors and ligand-gated ionotropic receptors present on the postsynaptic neuronal cells.[1−3] The metabotropic Glu receptor subtype 5 ($mGluR_5$) is known to be actively involved in modulating excitatory signals via a heterogeneous family of G-protein-coupled receptors that are activated by Glu.[4,5] An imbalance of Glu concentration and loss of their corresponding receiving $mGluR_5$ in the synaptic cleft have been implicated in a number of CNS disorders, such as pain, anxiety, depression, Parkinson's disease, and addiction.[1,4,6,7]

The *noninvasive* imaging of the brain using a powerful technique such as magnetic resonance imaging (MRI) [high spatial resolution imaging ($\leq$200 μm)] has revolutionized our understanding of the brain's organisational and operational complexity.[8] MR imaging procedures can be substantially improved when applied in combination with paramagnetic contrast agents (CAs) to enhance sensitivity and image quality. Gadolinium (Gd^{3+})-based CAs are used because of their high spin paramagnetism and the slow electronic relaxation of Gd^{3+}, which influence the longitudinal and transverse relaxation times (T_1 and T_2) of surrounding water protons, thereby altering the image contrast during MR measurements.[9] The use of nonspecific CAs show enhanced sensitivity and image quality, thereby improving the accuracy of prognoses in clinical applications. The sensitivity and specificity of imaging can be augmented several fold by introduction of "responsive CAs (RCAs)". These agents respond to changes in their surroundings by sensing changes in the biochemical environment, following spatially localized neural activation. In principle, these RCAs may exhibit relaxivity change by modulation of three parameters: (i) the number of water molecules bound directly to the gadolinium ion (q); (ii) the

Received: September 23, 2013
Revised: November 19, 2013
Published: November 19, 2013

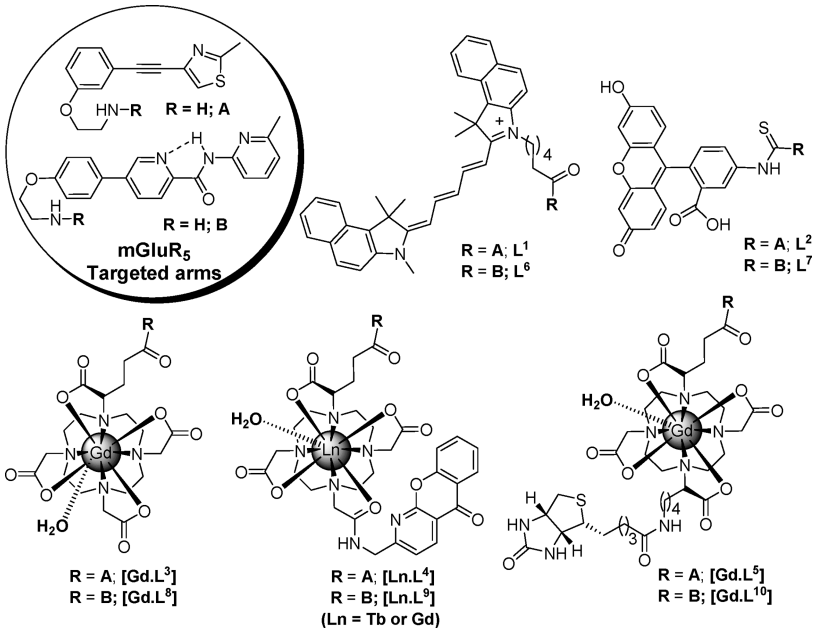

Figure 1. Structures of the imaging probes examined in this study.

Scheme 1. [a]

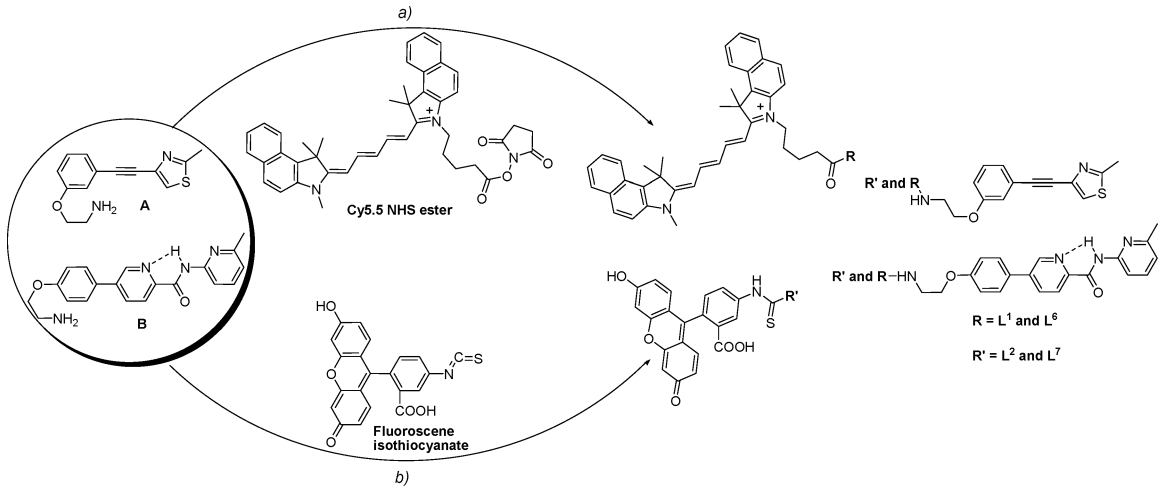

[a]Reagents, conditions, and yields: (a) DIPEA, DMF, RT, 18-22%; (b) H_2O, pH = 8, RT, 32-41%.

water exchange rate (k_{ex}); and (iii) the molecular rotational correlation time (τ_R). These changes can be detected and quantified by MRI.[9] We and others have published reports of pH, enzyme, and Ca^{2+} sensitive RCAs, for example.[10,11]

A key challenge in neuroimaging is to develop appropriate 'chemical tools' for MRI to detect synaptic glutamate fluctuations *noninvasively*. One approach could be to target Glu directly, by making small chemical entities. The design of such chemical entities is hampered by low selectivity toward Glu in comparison to similar amino acids such as aspartate or glutamine. In our approach, we follow an indirect path and target $mGluR_5$ located on the *postsynaptic* membranes that are modulated by glutamate upon neuronal firing. In order to devise a probe that functionally reports the Glu fluctuation, it is important that even during signal transduction the probe should mainly remain on the membrane surface bound to the receptors and not be internalized by receptor-mediated endocytosis.

Recently, we introduced a new set of chemical tools based on an antagonistic approach to target $mGluR_5$ and detect changes in glutamate concentration.[12] The results from a functional cellular calcium assay (potent antagonistic effects; 3.9 ± 0.9 and 3.1 ± 0.3, respectively) and the enhancement of receptor mediated cellular relaxation rates ($R_{1,cell}$ = 32% and 28%, respectively) at 3T revealed that two MRI probes ([**Gd.L**$^{3\ and\ 8}$]) (Figure 1) specifically interacted with cellular $mGluR_5$.[13] However, the observed increase in $R_{1,cell}$ could also result from internalization of the complex, via receptor-mediated endocytosis. Probe−receptor interaction assays at low temperature using MRI suggested that the probe interacted with cell surface receptors but may also have been taken up into cells.[13] Nonetheless, there is no direct proof to confirm that the compound is indeed specifically interacting with $mGluR_5$ on the live cell surface and is not getting internalized in cells through receptor-mediated endocytosis. Furthermore, due to the intrinsic insensitivity of MR imaging compared to optical

dx.doi.org/10.1021/cn400175m | *ACS Chem. Neurosci.* 2014, 5, 128−137

Scheme 2. [a]

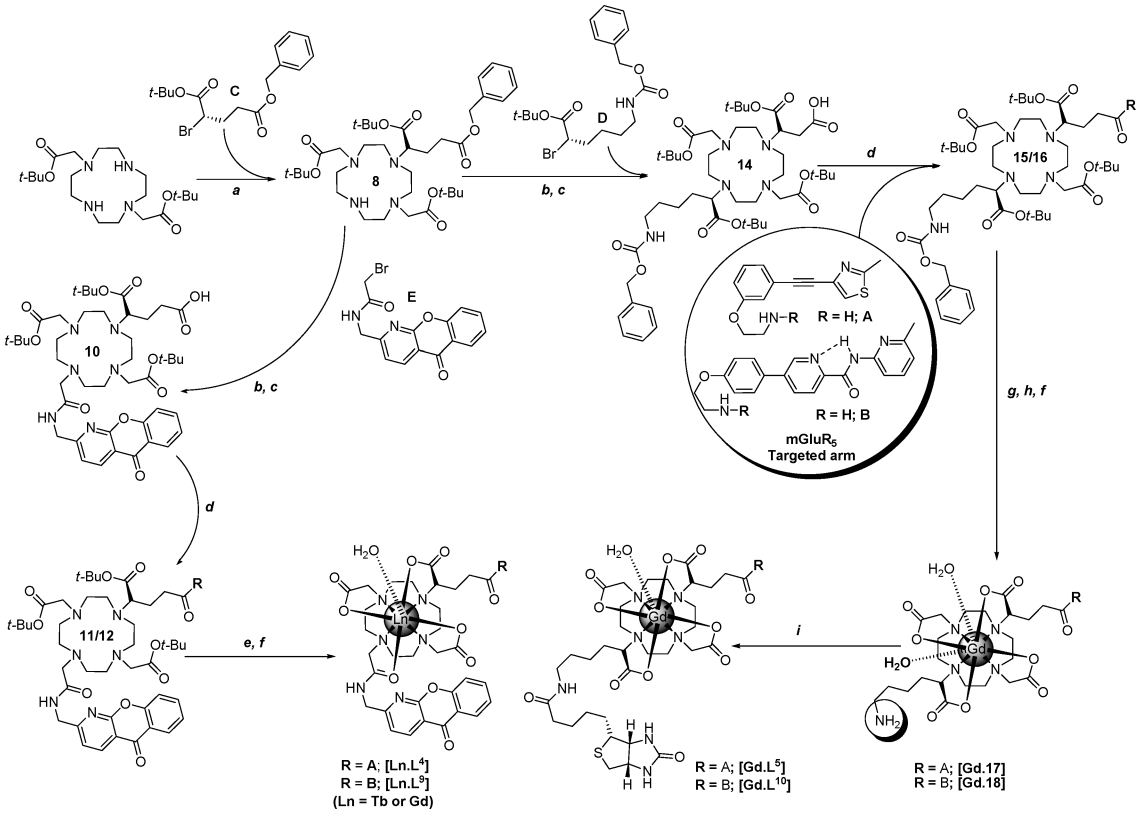

[a]Reagents, conditions, and yields : (a) Na_2CO_3, MeCN, 60°C, 40%; (b) K_2CO_3, MeCN, 80°C, 30−40%; (c) NaOH, H_2O:MeOH (1:9), RT; (d) **A**/**B**, HOBt, NMM, EDC, DMF, RT, 20−28%; (e) **11**/**12**/**17**/**18**, CH_2Cl_2:TFA (1:9), RT; (f) $\mathbf{L^4}$/$\mathbf{L^9}$/**17**/**18**, $LnCl_3.6H_2O$ (Ln^{3+}=Gd^{3+}/Tb^{3+}), H_2O, pH 5.5, 80°C; (g) (i) **15**, 0.15 M $Ba(OH)_2$, glyme, H_2O, 80°C, (ii) CH_2Cl_2:TFA (1:9), RT, 78%; (h) (i) **16**, 10% PdC, MeOH, 40 psi, RT, (ii) CH_2Cl_2:TFA (1:9), RT, 65%; (i) D-biotin, HATU, DIPEA, DMF, RT, 15−22%.

imaging, it is impossible to visualize the complexes [$\mathbf{Gd.L^{3\ and\ 8}}$] directly in/on cells. Hence, a series of bifunctional imaging probes was designed to allow real-time visualization of the live cell surface receptors, using high-resolution fluorescence microscopic methods (Figure 1).

RESULTS AND DISCUSSION

Synthesis of Bifunctional Imaging Probes. In order to allow the direct visualization of the cell surface $mGluR_5$, we designed characterized and evaluated three sets of imaging probes (fluorescently labeled [$\mathbf{L^{1,2,6\ and\ 7}}$] and MRI probes [$\mathbf{Gd.L^{4-5\ and\ 9-10}}$] (Figure 1). These probes were synthesized using alkyne and dipyridyl amide derived antagonistic amines [**A** and **B**]. These amine precursors were synthesized using a range of standard synthetic transformations including Suzuki/Sonogashira coupling, alkylation, amide formation, protection, and deprotection (Supporting Information Scheme S1).

The four fluorescent probes [$\mathbf{L^{1,2,6\ and\ 7}}$] were synthesized using either cyanine 5.5 NHS ester with Hünig's base in DMF or fluorescein isothiocyanate at pH 8−8.5 in water, in single step conjugation reactions with the antagonistic amines, **A** and **B** (Scheme 1). In FITC conjugation, the pH was not allowed to exceed 8.5 because at pH > 9, lactone cleavage of the FITC part occurs, leading to the formation of a side product.

The azaxanthone based antagonistic lanthanide complexes, [$\mathbf{Ln.L^{4\ and\ 9}}$], were synthesized as depicted in Scheme 2. Alkylation of the *tert*-butyl ester of 1,7-bis(carboxymethyl)-1,4,7,10-tetraazacyclododecane (DO2A) by the (*S*)-5-benzyl 1-*tert*-butyl 2-bromopentanedioate (**C**)[14] yielded the protected DO2A-GA (**8**). Subsequent treatment of **8** with 2-bromo-*N*-((5-oxo-5*H*-chromeno[2,3-*b*]pyridin-2-yl)methyl)acetamide (**E**) and Hünig's base in anhydrous MeCN yielded tetrasubstituted intermediate **9**, from which the carboxylic acid **10** was obtained following basic hydrolysis of the benzyl group. The azaxanthone bromoamide (**E**) was synthesized via alkylation of 2-(aminomethyl)-5-*H*-chromeno[2,3-*b*]pyridin-5-one[14] (as previously reported) with 2-bromoacetyl bromide in MeCN. The acid, **10**, was coupled with the amines **A** and **B**, using *N*′-(3-dimethylaminopropyl)-*N*-ethylcarbodiimide (EDC), 1-hydroxybenzotriazole (HOBt), and *N*-methylmorpholine (NMM) in DMF, to afford the protected amides, **11** and **12**, respectively. Following removal of the ester groups with TFA, the desired lanthanide complexes, [$\mathbf{Ln.L^{4\ and\ 9}}$], were formed by treatment with $LnCl_3{\cdot}6H_2O$ (Gd^{3+} and Tb^{3+}) at pH 6.5.

The biotin coupled antagonistic gadolinium complexes, [$\mathbf{Gd.L^{5\ and\ 10}}$], were synthesized in 7 steps as shown in Scheme 2. Alkylation of **8** with (*S*)-*tert*-butyl 6-(benzyloxycarbonylamino)-2-bromohexanoate (**D**)[15] gave the compound **13**, which was further treated with base, cleaving the benzyl group to afford the acid **14**. The tetraesters **15** and **16** were synthesized by coupling the amines **A**/**B** and acid **14** by using standard carbodiimide methodology [EDC/HOBt/NMM]. The intermediate amines, **17** and **18**, were obtained by successive deprotections (benzylcarbamate removal by 0.15 M $Ba(OH)_2$, glyme for alkyne amine; hydrogenation using PdC as the catalyst for dipyridyl amine and *tert*-butyl groups with

dx.doi.org/10.1021/cn400175m | ACS Chem. Neurosci. 2014, 5, 128−137

CH_2Cl_2:TFA). Ligands **17** and **18** were loaded with Gd^{3+} using $GdCl_3 \cdot 6H_2O$ in water at pH 6.5. The amines of **Gd.17** and **Gd.18** were coupled to the carboxylic acid group of D-biotin, using HATU and DIPEA in DMF, to afford the final complexes [**Gd.L**$^{5 \text{ and } 10}$], respectively.

The final complexes [**Ln.L**$^{4 \text{ and } 9}$] and [**Gd.L**$^{5 \text{ and } 10}$] were purified by reverse phase HPLC, and the metal ion concentration of [**Tb.L**$^{4 \text{ and } 9}$] and [**Gd.L**$^{4,5 \text{ and } 9,10}$] was measured using Evans' bulk magnetic susceptibility measurements.[16] The longitudinal proton relaxivities (r_{1p}) of [**Gd.L**$^{4,5 \text{ and } 9,10}$] were measured in aqueous solution (pH 7.4) at 37 °C and 1.4 T, and found to be 7.49, 7.23, 7.98, and 7.88 mM^{-1} s^{-1}, respectively. Such values are slightly higher than those reported for related monoaqua gadolinium complexes, [9] as a consequence of their bigger molecular volume and slower rotational correlation time, coupled to a fast water exchange rate and a significant second sphere contribution to the overall relaxivity. The relative importance of this effect has been emphasized earlier.[17,18]

Biochemical Evaluation of Imaging Probes. *Cellular Receptor Expression and Cytotoxicity.* The *in vitro* receptor binding behavior of the newly modified imaging probes was investigated on cortical rat astrocytes that are known to express functional $mGluR_5$ abundantly.[19] Optical microscopy studies were undertaken with cultured $mGluR_5$ expressing secondary astrocytes (Supporting Information). The secondary astrocytes were obtained from frozen-harvested, confluent primary astrocyte cultures which were gently thawed and then recultured on surface-modified glass chamber slides (Supporting Information). The medium was changed after 24 h to allow the cells to attach to the chamber slide surface. Fresh G-5 supplement (Invitrogen) containing medium was used to increase the expression of $mGluR_5$,[20] and the cells were used for the microscopy studies after 4 days. The expression of $mGluR_5$ was confirmed by immunofluorescence staining methods (Supporting Information Figure S1).[12,13] *In vitro* MRI studies were done on primary astrocytes as explained earlier.[12,13] None of the imaging probes (up to 200 μM) induced any significant cytotoxicity on astrocytes after 24 h of incubation, as observed in a metabolic activity test for mitochondrial dehydrogenase activity (XTT assay) (data not shown).

Microscopic Techniques Used to Visualize $mGluR_5$ on Live Astrocytes. To investigate the cellular distribution of these imaging probes, two fluorescence imaging techniques have been used. Total internal reflection fluorescence (TIRF) microscopy was used to analyze the localization of the probes near the plasma membrane. Due to its experimental design, TIRF microscopy facilitates very shallow depth penetration and primarily illuminates the fluorophores near to the coverslip adhered cell surface; hence, the signal from intracellular regions is reduced to a minimum.[21] A signal from the imaging probes at a maximum distance of 150 nm from the plasma membrane could be obtained employing this microscopy technique. Using the same cell preparations, live-cell laser scanning confocal microscopy (LSCM) studies were also performed. Extracellular receptor tagging and/or intracellular localization of probes in the entire cell was observed. Depth profiling "z-stacks" were recorded, selectively scanning through well-defined subcellular sections of the cell. These z-stacks were subjected to three-dimensional reconstruction, in order to clearly depict the distribution of the imaging probes in/on the astrocytes.

Fluorescently Labeled Probes. In the first attempt to visualize $mGluR_5$ on live astrocytes, the first set of four optical probes [**L**$^{1 \text{ and } 6}$] (1 μM) and [**L**$^{2 \text{ and } 7}$] (10 μM) were incubated on cultured astrocytes for 15 or 45 min (37 °C, 5% CO_2). After incubation, the cells were washed twice with Hank's balanced salt solution (HBSS) to remove unbound material. The Cy5.5 conjugated probes, [**L**$^{1 \text{ and } 6}$] (Figure 1), showed a complete intracellular distribution in $mGluR_5$ expressing astrocytes. No signal was obtained in TIRF microscopy, but a punctate intracellular distribution was observed in epifluorescence mode (data not shown). The mitochondrial distribution of [**L**$^{1 \text{ and } 6}$] was confirmed using the commercial stain, MitoTracker (Invitrogen) (500 nM) and coincubation with [**L**$^{1 \text{ and } 6}$] (1 μM) (Supporting Information Figure S2). Such observations indicate that in this case the cellular distribution of the probes is not driven by the receptor binding moiety but instead is determined by the larger Cy5.5 fluorophore subunit. The structural and charge similarity of Cy5.5 to the mitochondrial dye may partly explain the intracellular distribution of the probes.

On the other hand, the fluorescein conjugated probes (Figure 1), [**L**$^{2 \text{ and } 7}$] (10 μM, 45 min), could be visualized on the cell surface of astrocytes using TIRF microscopy. However, by examining the epifluorescence images recorded by TIRF and the intracellular planes obtained from LSCM, it was confirmed that these probes were also present in intracellular regions (Supporting Information Figure S3). The conjugate **L**^{7} was brighter both on the cell surface and inside, consistent with better receptor binding/uptake of this probe compared to **L**^{2}. In the past, we[22−25] and others[26,27] have shown that a consequence of appending a membrane permeable (relatively lipophilic) fluorescent moiety can be to perturb cell-uptake mechanisms, thereby promoting nonspecific cell internalization of the probe. Therefore, these fluorescently labeled probes [**L**$^{1,2,6 \text{ and } 7}$] were not considered to be appropriate to visualize cell-surface $mGluR_5$ and therefore should not be compared with the MR performance of the parent probes [**Gd.L**$^{3 \text{ and } 8}$] that gave rise to the observed receptor mediated $R_{1,cell}$ enhancements.

Luminescent Probes Based on Terbium Emission. In an alternative approach, azaxanthone-based luminescent probes, [**Tb.L**$^{4 \text{ and } 9}$] (Figure 1), were designed to tag and visualize $mGluR_5$. In this set of imaging probes, we preserved the parent molecular structures [**Gd.L**$^{3 \text{ and } 8}$] and appended the luminophore on the *trans*-position of [**Gd.L**$^{3 \text{ and } 8}$] (i.e., about 10 Å away) to allow visualization by optical microscopy. Terbium(III) complexes of [**L**$^{4 \text{ and } 9}$] were incubated with cultured secondary astrocytes for either 10 or 45 min, using 10 or 100 μM loading concentrations, at 37 °C, 5% CO_2, and cells were washed twice with HBSS to remove any unbound probe that may be present. In order to present high quality microscopy images with adequate brightness and S/N ratio, for example, to compensate for lower probe emission/uptake, a 100 μM loading concentration at 45 min was finally used. The cellular localization profile of the complexes was observed by examining the terbium emission (450−570 nm) by fluorescence microscopy, following excitation of the azaxanthone chromophore at 355 nm. Optical sections through the cell were examined by LCSM, and confirmed that these two complexes were also distributed within the cell, consistent either with cell surface receptor mediated or nonspecific uptake (Supporting Information Figure S4).

In the past, we have identified that such amide-linked azaxanthone sensitizing moieties promote probe uptake into the cell by macropinocytosis.[28] We have also observed that small structural modifications to the chromophore of a family of emissive Tb^{3+} complexes have an influence on the cellular compartmentalization profile.[25,29] Therefore, by virtue of the lipophilic nature of the azaxanthone moiety, the distribution of these molecules may also not be directly compared to the behavior of the parent complexes, [**Gd.L**$^{3\text{ and }8}$].

Microscopic Visualization by Complex Conjugate Interactions Based on Biotin/Avidin. In order to target and visualize $mGluR_5$ on the cell surface selectively, we needed to perturb the parent MRI probe [**Gd.L**$^{3\text{ and }8}$] structure minimally, minimizing changes to complex charge and hydrophilicity. Accordingly, a final set of probe molecules [**Gd.L**$^{5\text{ and }10}$] was prepared, each being derived from 12 (N_4, C_8) membered macrocyclic ring, *tert*-butyl ester of *trans*-N^1,N^7-DO2A [(7-carbonylmethyl-1,4,7,10-tetraazacyclododec-1-yl)-acetic acid].

The probe structure retained the same linkage to the antagonists (**A** and **B**), and D-biotin was appended to the side chain lysine amine, linked to the *trans*-related ring nitrogen N^{10} of the macrocycle (Figure 1). This design was based on the hypothesis that if the cell-surface $mGluR_5$ binding is mainly responsible for the increase in $R_{1,cell}$ for [**Gd.L**$^{3\text{ and }8}$], the antagonistic moiety of the newly designed [**Gd.L**$^{5\text{ and }10}$] would interact with the cell specific receptors and the remote, *trans*-substituted biotin moiety would be available to bind to the emissive AvidinAlexaFluor488 (Invitrogen) to allow visualization of probe localization by optical microscopy techniques.

Secondary astrocytes expressing $mGluR_5$ were incubated with [**Gd.L**$^{5\text{ and }10}$] (100 μM, 10−45 min) and then washed with HBSS to remove the unbound probes. Following subsequent incubation with AvidinAlexaFluor488 (25 μM, 5 min, 37 °C, 5% CO_2), cells were washed with HBSS again to eliminate any unbound dye. These AvidinAlexaFluor488-[**Gd.L**$^{5\text{ or }10}$]-$mGluR_5$ tagged cells were imaged by both TIRF and LSCM. The TIRF images revealed a strong signal near the plasma membrane, consistent with receptor tagging; the punctate distribution resembled the pattern of the $mGluR_5$ distribution on the cell surface (Supporting Information Figures S1 and S5). The intracellular sections of these labeled astrocytes were imaged by LCSM, confirming the membrane binding of the probes. The intracellular regions of the cells were not significantly stained, even following a 45 min incubation (Supporting Information Figure S5). Further demonstration/visualization of the selective cell-surface labeling of [**Gd.L**$^{5\text{ and }10}$] was provided by examining a HCC projection (color coded topological depth map reconstruction from the recorded z-stacks (voxel size 120 × 120 × 780 nm^3) of the optical sections reconstructed topological surface map projection of the chosen 7 μm deep section of the scanned raster). A HCC projection allows the color coded depth profile information of all the sections to be projected onto one plane (Supporting Information Figure S6 and Videos S1 and S2). These studies also revealed that [**Gd.L**^{10}] labeled better at low concentrations (10 μM [**Gd.L**^{10}], 2.5 μM of AvidinAlexaFluor488) compared to [**Gd.L** ^{5}] (Supporting Information Figure S7).

In order to confirm the cell-surface tagging of $mGluR_5$, a detailed study with [**Gd.L** ^{10}] was undertaken. The nonspecific plasma membrane stain dye CellMask Orange was used, parallel with the nuclear blue stain dye, Hoechst 33342. The secondary astrocytes were sequentially incubated with [**Gd.L**^{10}] (10 μM, 10 min), AvidinAlexaFluor488 dye (2.5 μM, 5 min), CellMask Orange (5 $\mu g\ mL^{-1}$ for 5 min), and Hoechst 33342 (1 $\mu g\ mL^{-1}$ for 5 min). During successive incubation, the cells were washed twice with HBSS to remove unreactive compounds. The TIRF images displayed a uniform labeling of the plasma membrane by CellMaskOrange (Figure 2B), while the [**Gd.L**^{10}]-

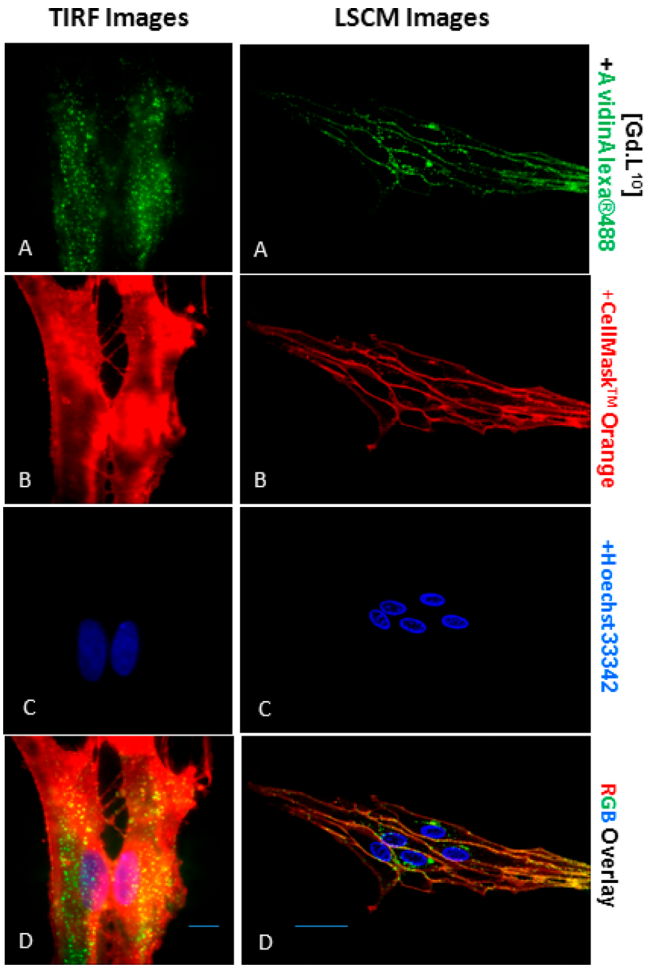

Figure 2. Detailed visualization of the cell surface using TIRF microscopy: (left column) and LSCM (right) of live $mGluR_5$ expressing secondary astrocytes after labeling with [**Gd.L**^{10}] (10 μM for 10 min), (A) Avidin Alexa-Fluor488 (green) (2.5 μM for 5 min), (B) CellMask Orange (red) (5 $\mu g\ mL^{-1}$ for 5 min), and (C) Hoechst 33342 (blue) (1 $\mu g\ mL^{-1}$ for 5 min). The figure shows the AvidinAlexa-Fluor488 conjugated to receptors labeled with [**Gd.L**^{10}], CellMask Orange staining of the cell membrane, and Hoechst 33342 labeling of cell nuclei. Hoechst images in TIRF (left column, C) were acquired in epifluorescence mode. (D) Overlay of (A), (B), and (C) images. Bar size is 11 μm in the TIRF images, and 30 μm in the LSCM images.

AvidinAlexaFluor488 conjugate exhibited a punctate cell surface localization (Figure 2A left). The images obtained by LSCM confirmed the results from the TIRF analysis, proving that the conjugate is predominantly located on the outside of the cell surface; significant intracellular staining was not observed by LCSM, only a few punctate perinuclear fluorescent conjugates (Figure 2A right). The Hoechst 33342 images were acquired in epifluorescence mode on the TIRF microscope to locate the nuclei in the astrocytes (Figure 2C left). An overlay of the

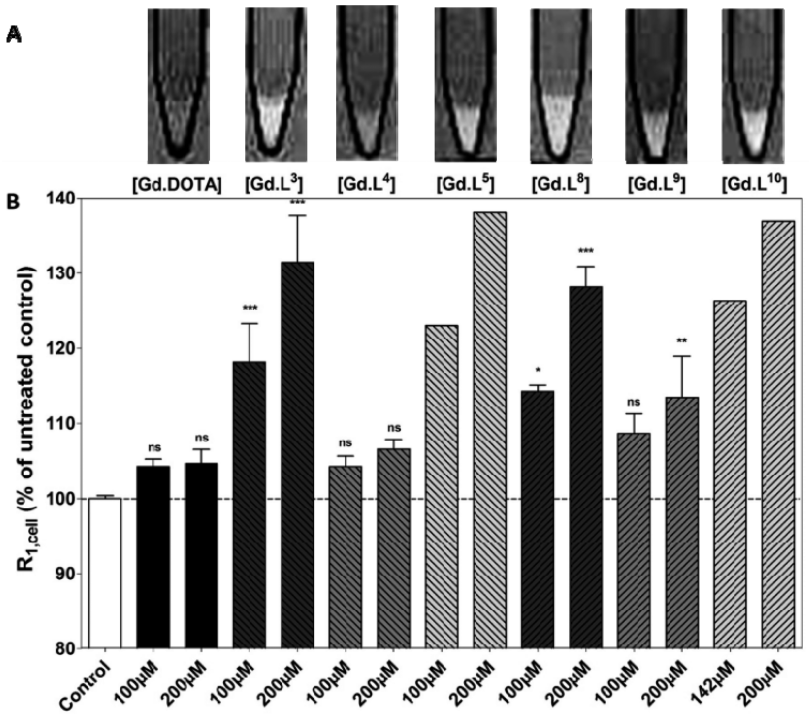

Figure 3. (A) T_1-weighted MR images of 1×10^7 untreated cells (control) and cells treated for 45 min with 200 μM [**Gd.DOTA**] or [**Gd.L**$^{3-5,8-10}$]. Images were recorded using a turbo spin echo sequence with a matrix of 256×256 voxels over a field of view of 110×110 mm^2, slice thickness of 1 mm resulting in a voxel size of $0.4 \times 0.4 \times 1.0$ mm^3, T_R 1000 ms, T_E 13 ms, T_i 23 ms, and 20 averages. (B) Cellular relaxation rates $R_{1,cell}$ of primary astrocytes after treating with increasing concentrations of [**Gd.DOTA**] or [**Gd.L**$^{3-5,\ 8-10}$] for 45 min. Control represents cells incubated with HBSS without CA. [**Gd.DOTA**] served as a negative control. Data are means of $n = 1-6 \pm$ SEM. $^*P < 0.05$, $^{**}P < 0.01$, $^{***}P < 0.001$ vs control. ANOVA with Bonferroni's multiple comparison post-test. Note: The concentrations for [**Gd.L**^{10}] were 142 and 200 μM.

LSCM image depicts the orange/green envelope of the plasma membrane, with the blue nuclei shown in the center (Figure 2D right).

Control Experiments. The specificity of the compounds toward $mGluR_5$ was also investigated by using $mGluR_5$-negative NIH-3T3 fibroblast cells. As described for the secondary astrocytes, sequential loading (equivalent amount and incubation time) of [**Gd.L**^{10}] and AvidinAlexaFluor488 dye were incubated with NIH-3T3 cells. No staining (cell surface or intracellular localization) was observed, strengthening the argument that receptor-mediated binding occurs only on the $mGluR_5$ (data not shown). In a further control experiment, the labeling of AvidinAlexaFluor488 on astrocytes did not show any localization using either microscopy technique (data not shown), emphasizing that this dye itself cannot be taken up by astrocytes. A preconjugated construct ([**Gd.L**$^{5 \text{ and } 10}$]-AvidinAlexaFluor488) also bound with $mGluR_5$ and no significant uptake in cells were observed (data not shown).

Cellular Receptor-MR Imaging Probes Studies in Cell Suspensions: Cellular ^{1}H-MR Relaxation Enhancement. The structural modification of the $mGluR_5$ parent MRI probes [**Gd.L**$^{3 \text{ and } 8}$][12,13] can have a profound effect on their receptor binding efficiency. Therefore, it was necessary to investigate the receptor binding behavior of these newly modified imaging probes [**Gd.L**^{4,5,9,10}] by MRI, comparing it with the performance of the parent complexes [**Gd.L**$^{3 \text{ and } 8}$]. Primary astrocytes were incubated with [**Gd.L**$^{3-5 \text{ and } 8-10}$] (100–200 μM probe concentrations, 45 min incubation time at 37 °C, 5% CO_2), washed with buffer to remove unbound molecules, and resuspended in fresh buffer, and subsequently, T_1-weighted images were recorded on a 3T Siemens human whole body MR scanner (Figure 3A). The T_1-weighted images were used to calculate cellular longitudinal relaxation rates $R_{1,cell}$, which represents cellular labeling (Figure 3B).[12,13] The complexes [**Gd.L**^{3}] and [**Gd.L**^{8}] showed statistically significant increases in $R_{1,cell}$, as indicated recently (Figure 3B).[13] Furthermore, the *trans*-substituted biotin probes [**Gd.L**^{5}] and [**Gd.L**^{10}] showed similar behavior (200 μM; increase in $R_{1,cell}$ = 38% and 36%, respectively) to that of the parent analogues ([**Gd.L**$^{3 \text{ and } 8}$]). The modulations in $R_{1,cell}$ ($R_1 = 1/T_1$) on interacting with $mGluR_5$ were attributed to slower molecular tumbling of the complex [increase in rotational correlation time (τ_R)] and fast water exchange rate with bulk water (k_{ex}) when bound to the cell surface receptors.[13]

The azaxanthone-based gadolinium probes, [**Gd.L**$^{4 \text{ and } 9}$] behaved quite differently. No significant changes in $R_{1,cell}$ were observed with [**Gd.L**^{4}], whereas the higher concentration (200 μM) of [**Gd.L**^{9}] led to a small increase in $R_{1,cell}$ after 45 min of incubation, albeit to a lesser extent than its corresponding parent probe [**Gd.L**^{8}] (200 μM [**Gd.L**^{9}]: 113.5% of control vs 200 μM [**Gd.L**^{8}] with 128.2% of control). A significant loss in the apparent $R_{1,cell}$ of [**Gd.L**$^{4 \text{ and } 9}$] can be explained by reference to the luminescence studies of the corresponding Tb complexes [**Tb.L**$^{4 \text{ and } 9}$]. The lanthanide luminescence microscopy studies had shown the well-defined punctate vesicular distribution profile, possibly associated with lysosomal localization, as seen previously with Ln(III) complexes of related structure and overall complex charge.[23] Therefore, it is reasonable to speculate that confinement within vesicles restricts the exchange of water molecules that can access the paramagnetic metal center. Such a "relaxation quenching" effect has already been reported by Aime and co-

dx.doi.org/10.1021/cn400175m | *ACS Chem. Neurosci.* 2014, 5, 128–137

workers[30,31] and has been interpreted in terms of a three compartment relaxation model.[32]

SUMMARY AND CONCLUSIONS

In conclusion, we have developed probes that specifically target $mGluR_5$ on astrocytes and have described the direct observation of cell surface receptor binding using optical imaging techniques. By employing a two-step approach, based on a remotely linked biotin−avidin interaction, the binding ability of the parent molecule was minimally perturbed and characterization by both MRI and optical methods was rendered possible.

The next step will focus on the use of longitudinal studies for testing these imaging probes using intracranial injection directly in the mouse brain to map the $mGlu_5$ receptor density. The blood-brain barrier (BBB) is the most crucial bottleneck in attaining molecular delivery through the blood capillaries. For further clinical application there is an obvious need for noninvasive delivery of diagnostic agents to the brain. An inability to enter the brain through the blood flow, either developing artificial methods for overcoming this barrier are required for such anionic complexes delivery in the brain or the successful RCAs could be conjugated with already established BBB permeating agents.[33] We will also extend these encouraging results by *noninvasively* mapping of $mGluR_5$ by MRI in depressed, anxiety, and drug-abuse mouse models. The potential development of medications for the treatment of addiction and other neuropsychiatric disorders, these imaging probes could also provide new pathological information of the brain.

Overall, these synthetic imaging probes could have importance not only in studying cell receptor distribution, but also in allowing the study of signaling and activation processes in the brain, by allocating specific regions of the brain to be monitored by MRI, following functional stimulation.

METHODS

Synthesis of Imaging Probes. *(S)-Di-tert-butyl 2,2′-(4-(1-tert-butoxy-5-(2-(3-((2-methylthiazol-4-yl)ethynyl)phenoxy)-ethylamino)-1,5-dioxopentan-2-yl)-10-(2-oxo-2-((5-oxo-5H-chromeno[2,3-b]pyridin-2-yl)methylamino)ethyl)-1,4,7,10-tetraaza-cyclododecane-1,7-diyl)diacetate (**11**).* A solution of **10** (0.2 g, 2.18 mmol), 2-[3-{(2-methylthiazol-4-yl)ethynyl}phenoxy]ethanamine (**A**) (57 mg, 2.18 mmol), NMM (0.06 mL, 4.32 mmol), and HOBt (32 mg, 2.4 mmol) in anhydrous DMF (2 mL) was stirred at 0−5 °C for 15 min, and then *N*′-(3-dimethylaminopropyl)-*N*-ethyl-carbodiimide [EDC] (47 mg, 2.40 mmol) was added. The reaction mixtures were stirred for 12 h at room temperature. The completion of reaction was verified by TLC. The solution was poured into water (20 mL) and extracted with EtOAc (3 × 20 mL). The combined organic layers were dried over anhydrous Na_2SO_4 and filtered, and the filtrate evaporated under reduced pressure. The residue was purified by column chromatography (silica gel, 10% MeOH in CH_2Cl_2, Rf = 0.15) to give **11** as a light yellow gum (53 mg, 22%). ^{1}H NMR (700 MHz, $CDCl_3$): δ 1.42 (s, 9H, 3 × CH_3), 1.44 (s, 9H, 3 × CH_3), 1.47 (s, 9H, 3 × CH_3), 2.01−2.20 (m, 2H, CH−CH_2), 2.23−2.40 (m, 2H, CH_2−CO−NH), 2.76 (s, 3H, CH_3), 2.79−3.60 (br. m, 22H, CO−C*H*, NH−CH_2, CO−CH_2, ring CH_2), 3.62−3.75 (m, 3H, CO−C*H*, NH−CH_2), 4.08 (t, *J* = 8.00 Hz, 2H, O−CH_2), 4.70 (d, *J* = 7.5 Hz, 2H, CH_2), 6.13 (br. s, 1H, N*H*), 6.87 (d, *J* = 8.5 Hz, 1H, H_{Ar}), 7.05 (s, 1H, H_{Ar}), 7.17 (d, *J* = 8.0 Hz, 1H, H_{Ar}), 7.19 (d, *J* = 8.0 Hz, 1H, H_{Py}), 7.25 (t, *J* = 8.0 Hz, 1H, H_{Ar}), 7.43 (d, *J* = 7.5 Hz, 1H, H_{Ar}), 7.59 (t, *J* = 8.0 Hz, 1H, H_{Ar}), 7.75 (s, 1H, SC*H*C), 7.78 (d, *J* = 7.5 Hz, 1H, H_{Ar}), 8.31 (t, *J* = 8.0 Hz, 1H, H_{Ar}), 8.64 (d, *J* = 7.5 Hz, 1H, H_{Py}), 9.73 (br. s, 1H, N*H*). ESI HRMS (±): calcd $C_{58}H_{76}N_8O_{11}S$, *m*/*z* 1093.5433 $[M+H]^+$; found, 1093.5453 $[M+H]^+$.

*(S)-Di-tert-butyl 2,2′-(4-(1-tert-butoxy-5-(2-(3-(6-(6-methylpyridin-2-ylcarbamoyl)pyridin-3-yl)phenoxy)ethylamino)-1,5-dioxopentan-2-yl)-10-(2-oxo-2-((5-oxo-5H-chromeno[2,3-b]pyridin-2-yl)-methylamino)ethyl)-1,4,7,10-tetraazacyclododecane-1,7-diyl)-diacetate (**12**).* A solution of **10** (0.17 g, 1.86 mmol), amine (**B**) (65 mg, 1.86 mmol), NMM (0.05 mL, 3.71 mmol), and HOBt (28 mg, 2.04 mmol) in anhydrous DMF (2 mL) was stirred at 0−5 °C for 15 min, and then EDC (40 mg, 2.04 mmol) was added. The reaction mixtures were stirred for 12 h at room temperature. The completion of reaction was verified by TLC. The solution was poured into water (20 mL) and extracted with EtOAc (3 × 20 mL). The combined organic layers were dried over anhydrous Na_2SO_4 and filtered, and the filtrate evaporated under reduced pressure. The residue was purified by column chromatography (silica gel, 10% MeOH in CH_2Cl_2, Rf = 0.15) to give **12** as a light yellow gum (61 mg, 22%). ^{1}H NMR (400 MHz, $CDCl_3$): δ 1.37 (s, 9H, 3 × CH_3), 1.44 (s, 9H, 3 × CH_3), 1.46 (s, 9H, 3 × CH_3), 1.92−2.03 (m, 2H, CH−CH_2), 2.18−2.36 (m, 2H, CH_2−CO−NH), 3.56 (s, 3H, CH_3), 2.64−3.88 (br. m, 22H, CO−C*H*, NH−CH_2, CO−CH_2, ring CH_2, CO−C*H*, NH−CH_2), 4.06 (t, *J* = 8.00 Hz, 2H, O−CH_2), 4.69 (d, *J* = 7.5 Hz, 2H, CH_2), 6.89 (d, *J* = 8.5 Hz, 1H, H_{Py}), 6.97 (d, *J* = 7.5 Hz, 2H, H_{Ar}), 7.30−7.40 (m, 5H, 5 × H_{Ar}, H_{Py}), 7.44 (s, 1H, N*H*), 7.46 (s, 1H, N*H*), 7.68 (t, *J* = 8.0 Hz, 1H, H_{Py}), 7.70 (t, *J* = 8.0 Hz, 1H, H_{Py}), 7.77 (d, *J* = 7.0 Hz, 1H, H_{Py}), 7.95 (d, *J* = 8.0 Hz, 1H, H_{Py}), 8.26 (d, *J* = 8.5 Hz, 1H, H_{Py}), 8.26 (d, J=8.5 Hz, 1H, H_{Ar}), 8.55 (d, *J* = 8.5 Hz, 1H, H_{Py}), 8.72 (s, 1H, H_{Py}), 10.61 (br. s., 1H, N*H*). ESI HRMS (±): calcd $C_{58}H_{76}N_8O_{11}S$, *m*/*z* 1183.6186 $[M+H]^+$; found, 1183.6221 $[M+H]^+$.

Common Synthesis of L^4 and L^9. Compounds **11**/**12** (1 equiv) were dissolved in TFA/CH_2Cl_2 (9:1 mL) and stirred overnight. The solvent was removed by evaporation and dried under reduced pressure.

(S)-2,2′-(4-(1-Carboxy-4-(2-(3-((2-methylthiazol-4-yl)ethynyl)-phenoxy)ethylamino)-4-oxobutyl)-10-(2-oxo-2-((5-oxo-5H-chromeno[2,3-b]pyridin-2-yl)methylamino)ethyl)-1,4,7,10-tetraaza-cyclododecane-1,7-diyl)diacetic Acid (L^4). $\mathbf{L^4}$ was obtained as an off-white sticky solid (13.5 mg, 32%). ^{1}H NMR (400 MHz, D_2O): δ 1.76−2.04 (m, 2H, CH−CH_2), 2.95−3.13 (m, 2H, CH_2−CO−NH), 3.21 (s, 3H, CH_3), 2.75−3.82 (br. m, 25H, CO−C*H*, NH−CH_2, CO−CH_2, CH_2 ring), 3.85−4.24 (m, 4H, CH_2-CO, NH−CH_2), 6.88 (d, *J* = 8.0 Hz, 1H, H_{Ar}), 7.02 (s, 1H, H_{Ar}), 7.20 (t, *J* = 8.0 Hz, 1H, H_{Ar}), 7.35−7.69 (m, 4H, H_{Ar}, H_{Py}), 7.81 (s, 1H, S−C*H*-C), 8.16 (t, *J* = 7.5 Hz 1H, H_{Ar}), 8.57 (d, *J* = 8.0 Hz, 1H, H_{Ar}), 8.78 (d, *J* = 7.5 Hz, 1H, H_{Py}). ESI LRMS (±): calcd $C_{46}H_{52}N_8O_{11}S$, *m*/*z* 925.3 $[M+H]^+$; found, 925.7 $[M+H]^+$.

(S)-2,2′-(4-(1-Carboxy-4-(2-(3-(6-(6-methylpyridin-2-ylcarbamoyl)pyridin-3-yl)phenoxy)ethylamino)-4-oxobutyl)-10-(2-oxo-2-((5-oxo-5H-chromeno[2,3-b]pyridin-2-yl)methylamino)-ethyl)-1,4,7,10-tetraazacyclododecane-1,7-diyl)diacetic Acid (L^9). $\mathbf{L^9}$ was obtained as an off-white sticky solid (15 mg, 29%). ^{1}H NMR (400 MHz, MeOD): δ 2.02−2.58 (m, 4H, CHCH_2CH_2CONH), 2.68 (s, 3H, CH_3), 2.72−4.02 (br. m, 27H, NH−CH_2, CO−C*H*, O−CH_2, CO−CH_2, ring CH_2), 4.37 (d, *J* = 7.5 Hz, 2H, CH_2), 6.89 (d, *J* = 8.5 Hz, 1H, H_{Py}), 7.13 (d, *J* = 7.5 Hz, 1H, H_{Py}), 7.31 (d, *J* = 7.5 Hz, 1H, H_{Py}), 7.35 (d, *J* = 8.5 Hz, 1H, H_{Ar}), 7.38 (t, *J* = 8.0 Hz, 1H, H_{Ar}), 7.48 (t, *J* = 8.0 Hz, 1H, H_{Py}), 7.57 (d, *J* = 8.5 Hz, 2H, H_{Ar}), 7.71 (d, *J* = 7.0 Hz, 2H, H_{Ar}), 7.92 (t, *J* = 7.5 Hz, 1H, H_{Ar}), 8.03 (d, *J* = 8.0 Hz, 1H, H_{Py}), 8.06 (d, *J* = 8.0 Hz, 1H, H_{Ar}), 8.10 (d, *J* = 8.0 Hz, 1H, H_{Py}), 8.48 (d, *J* = 8.5 Hz, 1H, H_{Py}), 8.75 (s, 1H, H_{Py}). ESI LRMS (+): calcd $C_{52}H_{58}N_{10}O_{12}S$, *m*/*z* 1015.2 $[M+H]^+$; found, 1015.5 $[M+H]^+$.

Common Synthesis of [Ln.L^4] and [Ln.L^9]. Gadolinium complexes [**Ln.L^4**] and [**Ln.L^9**] were prepared from corresponding solutions of the ligands $\mathbf{L^4}$/$\mathbf{L^9}$ (1 equiv) and solutions of $LnCl_3{\cdot}6H_2O$ (Ln^{3+} = Gd^{3+}, Tb^{3+}; 1.1 equiv). The reaction mixture was stirred at 60 °C for 20 h. The pH was periodically checked and adjusted to 6.0 using solutions of NaOH (1 M) and HCl (1 N) as needed. After completion, the reaction mixture was cooled down and passed through Chelex-100 to trap free Ln^{3+} ions, and the Ln^{3+}-loaded complexes were eluted. The fractions were dialyzed (500 MW cutoff; Spectra/Pro biotech cellulose ester dialysis membrane, Spectrum Laboratories) and lyophilized to obtain off-white solids. The absence of free Ln^{3+} was checked with xylenol orange indicator. These complexes were

characterized by ESI-LRMS in positive/negative modes, and the appropriate isotope pattern distributions for Ln^{3+} were recorded.

[Tb.L⁴]. ESI LRMS (−): calcd $C_{46}H_{49}N_8O_{11}STb$, *m/z* 1079.24 $[M-H]^-$; found, 1079.27 $[M-H]^-$.

[Gd.L⁴]. ESI LRMS (−): calcd $C_{46}H_{49}GdN_8O_{11}S$, *m/z* 1078.24 $[M-H]^-$; found, 1078.60 $[M-H]^-$. r_{1p} = 7.49 mM^{-1} s^{-1} (60 MHz, 310 K).

[Tb.L⁹]. ESI LRMS (−): calcd $C_{52}H_{55}N_{10}O_{12}Tb$, *m/z* 1169.32 $[M-H]^-$; found, 1169.69 $[M-H]^-$.

[Gd.L⁹]. ESI LRMS (−): calcd $C_{52}H_{55}GdN_{10}O_{12}$, *m/z* 1168.32 $[M-H]^-$; found, 1168.74 $[M-H]^-$. r_{1p} = 7.98 mM^{-1} s^{-1} (60 MHz, 310 K).

*Di-tert-butyl 2,2′-(4-((R)-6-(benzyloxycarbonylamino)-1-tert-butoxy-1-oxohexan-2-yl)-10-((S)-1-tert-butoxy-5-(2-(3-((2-methylthiazol-4-yl)ethynyl)phenoxy)ethylamino)-1,5-dioxopentan-2-yl)-1,4,7,10-tetraazacyclododecane-1,7-diyl)diacetate (**15**)*. A solution of **14** (90 mg, 0.96 mmol), 2-[3-{(2-methylthiazol-4-yl)ethynyl}-phenoxy]ethanamine (**A**) (25 mg, 0.96 mmol), NMM (0.028 mL, 1.98 mmol), and HOBt (15 mg, 1.11 mmol) in anhydrous DMF (1 mL) was stirred at 0−5 °C for 15 min, and then EDC (22 mg, 1.11 mmol) was added. The reaction mixtures were stirred for 18 h at room temperature. The completion of reaction was verified by TLC. The solution was poured into water (20 mL) and extracted with EtOAc (3 × 20 mL). The combined organic layers were dried over anhydrous Na_2SO_4 and filtered, and the filtrate evaporated under reduced pressure. The residue was purified by column chromatography (silica gel, 10% MeOH in CH_2Cl_2, Rf = 0.35) to give **11** as a light yellow gum (22 mg, 20%). ^{1}H NMR (400 MHz, $CDCl_3$): δ 1.19−1.36 (m, 4H, CH_2), 1.38 (s, 9H, 3 × CH_3), 1.41 (s, 9H, 3 × CH_3), 1.43 (s, 9H, 3 × CH_3), 1.44 (s, 9H, 3 × CH_3), 1.84−2.62 (m, 6H, CH_2), 2.72 (s, 3H, CH_3), 2.73−3.55 (br. m, 23H, CO−C*H*, NH−CH_2, CO−CH_2, ring CH_2), 3.58−3.77 (m, 3H, CO−C*H*, NH−CH_2), 4.02 (t, *J* = 8.00 Hz, 2H, O−CH_2), 5.06 (s, 2H, CH_2), 6.19 (br. s, 1H, N*H*), 6.34 (br. s., 1H, N*H*), 6.88 (d, *J* = 9.0 Hz, 1H, H_{Ar}), 7.04 (s, 1H, H_{Ar}), 7.14 (t, *J* = 8.5 Hz, 1H, H_{Ar}), 7.24 (d, *J* = 9.0 Hz, 1H, H_{Ar}), 7.27−7.35 (m, 5H, H_{Ar}), 7.37 (s, 1H, C−C*H*-S). ^{13}C NMR (101 MHz, $CDCl_3$): δ 19.1, 23.1, 26.4, 27.6, 27.7, 28.2, 29.2, 32.5, 32.6, 38.8, 43.6, 53.3, 54.9, 55.6, 55.9, 58.1, 66.3, 66.6, 68.8, 69.9, 81.8, 82.0, 82.3, 83.3, 88.4, 115.5, 117.0, 122.4, 123.5, 124.6, 128.4, 129.5, 134.9, 136.6, 144.1, 156.5, 158.1, 165.7, 170.5, 172.8, 173.4, 174.8. ESI HRMS (±): calcd $C_{61}H_{91}N_7O_{13}S$, *m/z* 1146.6519 $[M+H]^+$; found, 1146.6498 $[M+H]^+$.

*Di-tert-butyl 2,2′-(4-((R)-6-(benzyloxycarbonylamino)-1-tert-butoxy-1-oxohexan-2-yl)-10-((S)-1-tert-butoxy-5-(2-(3-(6-(6-methylpyridin-2-ylcarbamoyl)pyridin-3-yl)phenoxy)ethylamino)-1,5-dioxopentan-2-yl)-1,4,7,10-tetraazacyclododecane-1,7-diyl)diacetate (**16**)*. A solution of **14** (90 mg, 0.96 mmol), 5-[4-(2-aminoethoxy)-phenyl]-*N*-(6-methylpyridin-2-yl)picolinamide (**B**) (35 mg, 0.96 mmol), NMM (0.028 mL, 1.98 mmol), and HOBt (15 mg, 1.11 mmol) in anhydrous DMF (1 mL) was stirred at 0−5 °C for 15 min, and then EDC (22 mg, 1.11 mmol) was added. The reaction mixtures were stirred for 18 h at room temperature. The completion of reaction was verified by TLC. The solution was poured into water (20 mL) and extracted with EtOAc (3 × 20 mL). The combined organic layers were dried over anhydrous Na_2SO_4 and filtered, and the filtrate evaporated under reduced pressure. The residue was purified by column chromatography (silica gel, 10% MeOH in CH_2Cl_2, Rf = 0.4) to give **11** as a light yellow gum (31 mg, 25%). ^{1}H NMR (700 MHz, $CDCl_3$): δ 1.19−1.39 (m, 4H, CH_2), 1.44 (s, 9H, 3 × CH_3), 1.45 (s, 9H, 3 × CH_3), 1.47 (s, 9H, 3 × CH_3), 1.48 (s, 9H, 3 × CH_3), 1.95−2.11 (m, 2H, CH_2), 2.13−2.27 (m, 2H, CH_2), 2.33 (t, *J* = 8.00 Hz, 2H, CH_2), 2.53 (s, 3H, CH_3), 2.71−3.52 (br. m, 23H, CO−C*H*, NH−CH_2, CO−CH_2, ring CH_2), 3.58−3.77 (m, 3H, CO−C*H*, NH−CH_2), 4.12 (t, *J* = 8.00 Hz, 2H, CH_2), 4.84 (br. s., 1H, N*H*), 5.09 (s, 2H, CH_2), 6.55 (br. s., 1H, N*H*), 6.94 (d, *J* = 7.5 Hz, 1H, H_{Py}), 7.08 (d, *J* = 8.50 Hz, 2H, H_{Ar}), 7.28−7.37 (m, 5H, H_{Ar}), 7.57 (d, *J* = 8.50 Hz, 2H, H_{Ar}), 7.66 (t, *J* = 8.00 Hz, 1H, H_{Py}), 8.03 (d, *J* = 8.00 Hz, 1H, H_{Py}), 8.25 (d, *J* = 8.00 Hz, 1H, H_{Py}), 8.30 (d, *J* = 8.00 Hz, 1H, H_{Py}), 8.80 (s, 1H, H_{Py}), 10.49 (br. s., 1H, N*H*). ^{13}C NMR (176 MHz, $CDCl_3$): δ 24.1, 24.3, 26.4, 27.8, 28.0, 28.1, 29.2, 31.7, 34.9, 36.4, 38.5, 52.6, 53.4, 55.9, 60.4, 61.1, 66.4, 66.5, 68.3, 69.4, 81.8, 81.9, 82.0, 82.3, 110.7, 115.5, 119.2, 122.4, 128.1, 128.3, 128.5, 134.9, 135.5, 136.5, 138.5, 139.2, 146.1, 147.2, 150.5, 156.3, 157.0, 159.5, 162.6, 172.8, 172.8, 173.1, 174.7, 175.1. ESI HRMS (±): calcd $C_{67}H_{97}N_9O_{13}$, *m/z* 1236.7278 $[M+H]^+$; found, 1236.7267 $[M+H]^+$.

*2,2′-(4-((R)-5-Amino-1-carboxypentyl)-10-((S)-1-carboxy-4-(2-(3-((2-methylthiazol-4-yl)ethynyl)phenoxy)ethylamino)-4-oxobutyl)-1,4,7,10-tetraazacyclododecane-1,7-diyl)diacetic Acid (**17**)*. A solution of **15** (20 mg, 0.18 mmol) in H_2O (1 mL), 0.15 M $Ba(OH)_2$ (0.06 mL, 0.54 mmol), and glyme (5 mL) was stirred at 60 °C for overnight. The reaction mixture was evaporated under reduced pressure. The crude intermediate product was dissolved in TFA/CH_2Cl_2 (9:1 mL) and stirred overnight. The solvent was removed by evaporation and dried under reduced pressure to give **17** as a yellow gum (10.9 mg, 78%). ^{1}H NMR (700 MHz, MeOD): δ 1.48−1.64 (m, 2H, CH_2), 1.68−2.01 (m, 4H, CH_2), 2.04−2.19 (m, 2H, CH_2CO−NH), 2.71 (s, 3H, CH_3), 2.90−3.40 (br. m, 22H, ring CH_2, CO−C*H*, CH_2−NH_2, CH−CH_2), 3.47−3.53 (m, 2H, CO−NH−CH_2), 3.54−3.61 (m, 4H, CH_2−CO), 4.05 (t, *J* = 8.00 Hz, 2H, O−CH_2), 6.96−7.04 (m, 1H, H_{Ar}), 7.06−7.17 (m, 2H, H_{Ar}), 7.29 (t, *J* = 8.0 Hz, 1H, H_{Ar}), 7.64 (s, 1H, C−C*H*-S). ESI LRMS (+): calcd $C_{37}H_{53}N_7O_{10}S$, *m/z* 788.3 $[M+H]^+$; found, 788.5 $[M+H]^+$.

*2,2′-(4-((R)-5-Amino-1-carboxypentyl)-10-((S)-1-carboxy-4-(2-(3-(6-(6-methylpyridin-2-ylcarbamoyl)pyridin-3-yl)phenoxy)-ethylamino)-4-oxobutyl)-1,4,7,10-tetraazacyclododecane-1,7-diyl)-diacetic Acid (**18**)*. A solution of **16** (30 mg, 0.24 mmol), (10%) Pd−C (1/5, w/w) in MeOH (5 mL) under H_2 (40 psi) was stirred at room temperature in a Parr apparatus for 4 h. The reaction mixture was filtered through Celite, and the filtrate evaporated under reduced pressure. The crude intermediate product was dissolved in TFA/CH_2Cl_2 (9:1 mL) and stirred overnight. The solvent was removed by evaporation and dried under reduced pressure to give **18** as a yellow gum (14.3 mg, 65%). ^{1}H NMR (700 MHz, MeOD): δ 1.40−1.55 (m, 2H, CH_2), 1.60−1.73 (m, 2H, CH_2), 1.77−1.90 (m, 2H, CH_2), 1.93−2.08 (m, 2H, CH_2), 2.19−2.38 (m, 2H, CH_2), 2.44 (s, 3H, CH_3), 2.70−3.47 (br. m, 24H, CO−C*H*, NH−CH_2, CO−CH_2, ring CH_2), 3.48−3.67 (m, 2H, NH−CH_2), 4.02 (t, *J* = 8.00 Hz, 2H, O−CH_2), 6.84 (d, *J* = 8.0 Hz, 1H, H_{Py}), 7.03 (d, *J* = 8.0 Hz, 2H, H_{Ar}), 7.63 (d, *J* = 8.0 Hz, 2H, H_{Ar}), 7.76 (t, *J* = 7.5 Hz, 1H, H_{Py}), 8.10 (d, *J* = 8.00 Hz, 1H, H_{Py}), 8.13 (d, *J* = 8.00 Hz, 1H, H_{Py}), 8.14 (d, *J* = 8.00 Hz, 1H, H_{Py}), 8.87 (s, 1H, H_{Py}). ESI LRMS (+): calcd $C_{43}H_{59}N_9O_{11}$, *m/z* 878.4 $[M+H]^+$; found, 878.5 $[M+H]^+$.

*Common Synthesis of Gadolinium Complexes [**Gd.17**] and [**Gd.18**]*. Gadolinium complexes [**Gd.17**] and [**Gd.18**] were prepared from corresponding solutions of the ligands **17**/**18** (1 equiv) and solutions of $GdCl_3{\cdot}6H_2O$ (1.1 equiv). The reaction mixture was stirred at 60 °C for 20 h. The pH was periodically checked and adjusted to 6.0 using solutions of NaOH (1 M) and HCl (1 N) as needed. After completion, the reaction mixture was cooled down and passed through Chelex-100 to trap free Gd^{3+} ions, and the Gd^{3+}-loaded complexes were eluted. The fractions were dialyzed (500 MW cutoff; Spectra/Pro biotech cellulose ester dialysis membrane, Spectrum Laboratories) and lyophilized to obtain off-white solids. The absence of free Gd^{3+} was checked with xylenol orange indicator. These complexes were characterized by ESI-LRMS in positive/negative modes, and the appropriate isotope pattern distributions for Gd^{3+} were observed.

*[**Gd.17**]*. Yield =12 mg, 100% (an off white solid). ESI LRMS (+): calcd $C_{37}H_{49}GdN_7O_{10}S$, *m/z* 942.25 $[M+H]^+$ and 471.32 $[M+2H]^{2+}$; found, 942.79 $[M+H]^+$ and 471.98 $[M+2H]^{2+}$.

*[**Gd.18**]*. Yield = 17 mg, 100% (an off white solid). ESI LRMS (+): calcd $C_{43}H_{55}GdN_9O_{11}$, *m/z* 516.33 $[M+2H]^{2+}$; found, 516.55 $[M+2H]^{2+}$.

Common Synthesis of [Gd.L⁵] and [Gd.L¹⁰]. A solution of [**Gd.17**]/[**Gd.18**] (1 equiv), D-biotin (1.1 equiv), DIPEA (2 equiv), and HATU (1.1 equiv) in anhydrous DMF (1 mL) was stirred overnight at room temperature. The completion of reaction was verified by LRMS. The solution was evaporated under reduced pressure, purified by RP-HPLC, and lyophilized to obtain off-white solids.

[Gd.L⁵]. Yield = 3.26 mg, 22%. ESI-LRMS (±): calcd $C_{47}H_{63}GdN_9O_{12}S_2$, *m/z* 1166.32 $[M-H]^-$ and 584.32 $[M+2H]^{2+}$;

found, 1166.80 $[M-H]^-$ and 584.07 $[M+2H]^{2+}$, t_R = 12.6 min, r_{1p} = 7.23 mM^{-1} s^{-1} (60 MHz, 310 K).

[Gd.L[10]]. Yield = 3.1 mg, 15%. ESI-LRMS (±): $C_{53}H_{69}GdN_{11}O_{13}S$, m/z 1256.40 $[M-H]^-$ and 629.40 $[M+2H]^{2+}$; found, 1256.90 $[M-H]^-$ and 629.17 $[M+2H]^{2+}$, t_R = 12.9, r_{1p} = 7.88 mM^{-1} s^{-1} (60 MHz, 310 K).

Total Internal Reflection Fluorescence (TIRF) Microscopy. TIRF microscopy was performed on an inverted Leica TIRF MC Imaging system with excitation lasers set to 405, 488, and 561 nm to visualize Hoechst, GFP, and Cell mask, respectively. Acquisition was performed using an 100×/HCX Plan Apo Oil TIRF 1.47 objective. Imaging and image capture were performed using LASAFsoftware.

Confocal Microscopy. Cell images and colocalization experiments were obtained using a Leica SP5 II microscope. A HeNe laser was used to visualize SA-AF488 fluorescence. The microscope was equipped with a triple channel imaging detector, comprising two conventional PMT systems and a HyD hybrid avalanche photodiode detector. The latter part of the detection system, when operated in the BrightRed mode, is capable of improving imaging sensitivity above 550 nm by 25%, reducing signal-to-noise by a factor of 5. The pinhole was always determined by the Airy disc size, calculated from the objective in use (HCX PL APO 63×/1.40 NA LbdBlue), using the lowest excitation wavelength (488 nm). Scanning speed was adjusted to 400 Hz in a bidirectional mode, to ensure both sufficient light exposure and enough time to collect the emitted light from the optical probes (1024 × 1024 frame size, a pixel size of 120 × 120 nm and depth of 0.89 μm). The three-dimensional reconstruction was achieved using a novel saturation elimination algorithm update of the existing ImageJ 1.46r 3D plug-in using LSCM images recorded on the above detailed Leica SP5 II microscope. In these z-stack images, a deliberate 20% overlap in the applied axial resolution was introduced, determined by the applied optics and experimental parameters detailed above.

■ ASSOCIATED CONTENT

Supporting Information

Synthesis of intermediate amines A and B, experimental methods, Figures S1−S7, and Videos S1 and S2. This material is available free of charge via the Internet at http://pubs.acs.org.

■ AUTHOR INFORMATION

Corresponding Authors

*Fax: +49-8931872017. E-mail: anurag.mishra@helmholtz-muenchen.de (A.M.).

*E-mail: david.parker@durham.ac.uk (D.P.).

Present Address

[‖]A.M. and S.G.: Institute for Biological and Medical Imaging, Helmholtz Zentrum München (GmbH), Neuherberg 85764, Germany.

Author Contributions

A.M. conceived the project with D.P.'s consultancy. A.M. and N.S. performed the designing, chemical synthesis and characterisation of imaging probes. R.M., A.M., S.G., and R.P. performed the cell culture experiments, microscopic studies, and MRI experiments for the characterisation of the imaging probes. J.E., M.G., and D.P. supported the research. All authors analyzed the data and wrote the paper.

Funding

This work was supported by a Marie Curie Intra European Fellowship (PIEF-GA-2009-237253) [A.M.], the ERC (FCC266804) [A.M., N.S., R.P.], by the Biotechnology and Biological Sciences Research Council (BBSRC), UK (BB/G011818/1) [R.M.], the Ministry for Education and Research, BMBF (FKZ:01EZ0813) [S.G.], and the Max Planck Society.

Notes

The authors declare no competing financial interest.

■ ACKNOWLEDGMENTS

The authors would like to thank Dr. Tim Hawkins for his technical assistance.

■ REFERENCES

(1) von Bohlen und Halbach, O., and Dermietzel, R. (2006) *Neurotransmitters and Neuromodulators*, Wiley-VCH, Weinheim, Germany.

(2) Featherstone, D. E., and Shippy, S. A. (2008) Regulation of synaptic transmission by ambient extracellular glutamate. *Neuroscientist 14*, 171−181.

(3) Rothstein, J. D. (2000) Neurobiology. Bundling up excitement. *Nature 407*, 141−143.

(4) Rousseaux, C. G. (2008) A Review of Glutamate Receptors II: Pathophysiology and Pathology. *J. Toxicol. Pathol. 21*, 133−173.

(5) Conn, P. J., and Pin, J. P. (1997) Pharmacology and functions of metabotropic glutamate receptors. *Annu. Rev. Pharmacol. 37*, 205−237.

(6) Cleva, R. M., and Olive, M. F. (2011) Positive Allosteric Modulators of Type 5 Metabotropic Glutamate Receptors ($mGluR_5$) and Their Therapeutic Potential for the Treatment of CNS Disorders. *Molecules 16*, 2097−2106.

(7) Ferraguti, F., and Shigemoto, R. (2006) Metabotropic glutamate receptors. *Cell Tissue Res. 326*, 483−504.

(8) Logothetis, N. K., Guggenberger, H., Peled, S., and Pauls, J. (1999) Functional imaging of the monkey brain. *Nat. Neurosci. 2*, 555−562.

(9) Merbach, A. E., and Toth, E. (2001) *The Chemistry of Contrast Agents in Medical Magnetic Resonance Imaging*, Wiley, New York, Chichester.

(10) Bonnet, C. S., and Toth, E. (2010) MRI probes for sensing biologically relevant metal ions. *Future Med. Chem. 2*, 367−384.

(11) Mishra, A., Logothetis, N. K., and Parker, D. (2011) Critical *in vitro* evaluation of responsive MRI contrast agents for calcium and zinc. *Chem.—Eur. J. 17*, 1529−1537.

(12) Mishra, A., Gottschalk, S., Engelmann, J., and Parker, D. (2012) Responsive imaging probes for metabotropic glutamate receptors. *Chem Sci 3*, 131−135.

(13) Gottschalk, S., Engelmann, J., Rolla, G. A., Botta, M., Parker, D., and Mishra, A. (2013) Comparative *in vitro* studies of MR imaging probes for metabotropic glutamate subtype-5 receptor targeting. *Org. Biomol. Chem. 11*, 6131−6141.

(14) Atkinson, P., Findlay, K. S., Kielar, F., Pal, R., Parker, D., Poole, R. A., Puschmann, H., Richardson, S. L., Stenson, P. A., Thompson, A. L., and Yu, J. H. (2006) Azaxanthones and azathioxanthones are effective sensitisers for europium and terbium luminescence. *Org. Biomol. Chem. 4*, 3708−3708.

(15) Vibhute, S. M., Engelmann, J., Verbic, T., Maier, M. E., Logothetis, N. K., and Angelovski, G. (2013) Synthesis and characterization of pH-sensitive, biotinylated MRI contrast agents and their conjugates with avidin. *Org. Biomol. Chem. 11*, 1294−1305.

(16) Corsi, D. M., Platas-Iglesias, C., van Bekkum, H., and Peters, J. A. (2001) Determination of paramagnetic lanthanide(III) concentrations from bulk magnetic susceptibility shifts in NMR spectra. *Magn. Reson. Chem. 39*, 723−726.

(17) Botta, M. (2000) Second coordination sphere water molecules and relaxivity of gadolinium(III) complexes: Implications for MRI contrast agents. *Eur. J. Inorg. Chem.*, 399−407.

(18) Aime, S., Botta, M., Parker, D., and Williams, J. A. G. (1996) Extent of hydration of octadentate lanthanide complexes incorporating phosphinate donors: Solution relaxometry and luminescence studies. *J. Chem. Soc., Dalton Trans.*, 17−23.

(19) Danial, N. N., Gramm, C. F., Scorrano, L., Zhang, C. Y., Krauss, S., Ranger, A. M., Datta, S. R., Greenberg, M. E., Licklider, L. J., Lowell, B. B., Gygi, S. P., and Korsmeyer, S. J. (2003) BAD and glucokinase reside in a mitochondrial complex that integrates glycolysis and apoptosis. *Nature 424*, 952−956.

(20) Peavy, R. D., Chang, M. S. S., Sanders-Bush, E., and Conn, P. J. (2001) Metabotropic glutamate receptor 5-induced phosphorylation

of extracellular signal-regulated kinase in astrocytes depends on transactivation of the epidermal growth factor receptor. *J. Neurosci. 21*, 9619−9628.
(21) Mattheyses, A. L., Simon, S. M., and Rappoport, J. Z. (2010) Imaging with total internal reflection fluorescence microscopy for the cell biologist. *J. Cell Sci. 123*, 3621−3628.
(22) Mishra, A., Pfeuffer, J., Mishra, R., Engelmann, J., Mishra, A. K., Ugurbil, K., and Logothetis, N. K. (2006) A new class of Gd-based DO3A-ethylamine-derived targeted contrast agents for MR and optical imaging. *Bioconjugate Chem. 17*, 773−780.
(23) Montgomery, C. P., Murray, B. S., New, E. J., Pal, R., and Parker, D. (2009) Cell-Penetrating Metal Complex Optical Probes: Targeted and Responsive Systems Based on Lanthanide Luminescence. *Acc. Chem. Res. 42*, 925−937.
(24) New, E. J., Duan, R., Zhang, J. Z., and Hambley, T. W. (2009) Investigations using fluorescent ligands to monitor platinum(IV) reduction and platinum(II) reactions in cancer cells. *Dalton Trans.*, 3092−3101.
(25) New, E. J., Parker, D., Smith, D. G., and Walton, J. W. (2010) Development of responsive lanthanide probes for cellular applications. *Curr. Opin. Chem. Biol. 14*, 238−246.
(26) Puckett, C. A., and Barton, J. K. (2008) Mechanism of Cellular Uptake of a Ruthenium Polypyridyl Complex. *Biochemistry 47*, 11711−11716.
(27) Puckett, C. A., and Barton, J. K. (2009) Fluorescein Redirects a Ruthenium-Octaarginine Conjugate to the Nucleus. *J. Am. Chem. Soc. 131*, 8738−8739.
(28) Smith, D. G., Law, G. L., Murray, B. S., Pal, R., Parker, D., and Wong, K. L. (2011) Evidence for the optical signalling of changes in bicarbonate concentration within the mitochondrial region of living cells. *Chem. Commun. 47*, 7347−7349.
(29) New, E. J., Congreve, A., and Parker, D. (2010) Definition of the uptake mechanism and sub-cellular localisation profile of emissive lanthanide complexes as cellular optical probes. *Chem. Sci. 1*, 111−118.
(30) Terreno, E., Geninatti Crich, S., Belfiore, S., Biancone, L., Cabella, C., Esposito, G., Manazza, A. D., and Aime, S. (2006) Effect of the intracellular localization of a Gd-based imaging probe on the relaxation enhancement of water protons. *Magn. Reson. Med. 55*, 491−497.
(31) Geninatti Crich, S., Cabella, C., Barge, A., Belfiore, S., Ghirelli, C., Lattuada, L., Lanzardo, S., Mortillaro, A., Tei, L., Visigalli, M., Forni, G., and Aime, S. (2006) *In vitro* and *in vivo* magnetic resonance detection of tumor cells by targeting glutamine transporters with Gd-based probes. *J. Med. Chem. 49*, 4926−4936.
(32) Strijkers, G. J., Hak, S., Kok, M. B., Springer, C. S., Jr., and Nicolay, K. (2009) Three-compartment T1 relaxation model for intracellular paramagnetic contrast agents. *Magn. Reson. Med. 61*, 1049−1058.
(33) Malakoutikhah, M., Teixido, M., and Giralt, E. (2011) Shuttle-mediated drug delivery to the brain. *Angew. Chem., Int. Ed. Engl. 50*, 7998−8014.